USPIO-Enhanced Dynamic MRI: Evaluation of Normal and Transplanted Rat Kidneys

Dewen Yang,[1] Qing Ye,[1] Mangay Williams,[1] Ying Sun,[2] Tom C.-C. Hu,[1] Donald S. Williams,[1] José M.F. Moura,[2] and Chien Ho[1]*

To evaluate first-pass renal perfusion with ultrasmall superparamagnetic iron oxide (USPIO) particles by MRI, 40 normal rats (20 Dark Agouti (DA) rats and 20 Brown Norway (BN) rats) and 16 transplanted rats (12 allografts and four isografts) were studied on day 4 post-transplantation with different USPIO doses (3.0–18.1 mg Fe/kg/body weight). All animals underwent 128 consecutive snapshot fast low-angle shot (FLASH) coronal dynamic studies in 43 s. In the normal rats, a larger maximum signal decrease (MSD) in the cortex and the outer medulla is observed with an increasing dose of USPIO particles ($P < 0.01$). No significant differences were observed between the right and left kidneys at all doses studied. Higher MSD, time of occurrence of MSD (t_{MSD}), and wash-in slope appear with higher doses of USPIO particles. The dynamic curves for DA rats show similar shapes when compared to those for BN rats. In the transplanted rats, allograft kidneys show lower MSD, longer t_{MSD}, and lower wash-in slope compared to those in the normal kidneys. Isograft kidneys show perfusion patterns similar to those of normal kidneys in the cortex and the outer medulla. Histopathology indicates acute vascular rejection in all allografts and normal kidney architecture in all isografts. The results clearly show good agreement between the renal graft perfusion measurements and histopathological changes associated with rejection. This work also introduces a new signal analysis methodology for the automatic detection of transplanted organ rejection. This method compares the dynamics of the intrarenal signal intensities for native and transplanted kidneys. A quantitative measurement to detect significant differences between these signals was developed, and showed that this technique exhibits good performance in identifying renal rejection. Magn Reson Med 46:1152–1163, 2001. © 2001 Wiley-Liss, Inc.

Key words: kidney; transplanted rat kidney; dynamic magnetic resonance imaging; MRI contrast agents; ultrasmall superparamagnetic iron oxide (USPIO) particles

Successful renal transplants have been performed since the early 1950s. Approximately 12000 renal transplants are performed in the United States annually (1). Kidney transplantation is now widely accepted as the treatment of choice for patients with end-stage renal disease since it offers the best prognosis, a superior quality of life, and improved rehabilitation. Graft survival rates now are more than 85%, 60–80%, and 40–50% at 1, 5, and 10 years,

respectively (1,2). However, the immunological reaction of rejection, especially the acute rejection that occurs in the first few weeks following surgery, as well as chronic graft rejection, is still one of the major causes of functional failure in organ transplantation. Renal biopsy plays a critical role in diagnosing kidney allograft rejection, but this procedure subjects patients to multiple risks, including bleeding and infection. In addition, the relatively small-needle biopsies that are typically obtained from these allografts are subject to sampling errors and may lead to over- or underestimation of the extent of inflammation in the entire graft.

Because of the prevalence of graft failure, a reproducible, repeatable, and noninvasive technique for the detection of acute renal rejection would be a valuable diagnostic tool in renal transplantation. Although scintigraphy is traditionally the primary method for evaluating functional abnormalities, color Doppler ultrasonography and gadolinium-enhanced MRI provide more anatomic details (3). Color Doppler ultrasonography is a valuable method in the detection of segmental infarction or large areas of cortical necrosis (4). However, superficial cortical blood flow cannot be evaluated, and alteration of echogenicity is inconsistent and not specific. Color Doppler ultrasonography is not sensitive enough in the diagnosis of superficial cortical necrosis or small peripheral perfusion defects, particularly in the case of hemorrhagic necrosis (3). Several early studies using T_1- and T_2-weighted spin-echo sequences and T_1-weighted gradient-echo sequences have been applied to analyze the graft status by assessing structural and anatomical changes. Allograft rejection results in an increase in the T_1 shortening of the renal cortex compared to that of the medulla, which is related to interstitial edema of the renal cortex. The loss of corticomedullary differentiation in T_1-weighted images has been reported as the most consistent MRI finding in the evaluation of acute rejection (5–7). However, some other studies have suggested that these findings were nonspecific, because the loss of corticomedullary differentiation could also be seen in acute tubular necrosis, cyclosporine toxicity, and infectious nephritis (8,9). Dynamic contrast-enhanced renal MRI has been shown to provide morphologic information comparable to computer tomography and ultrasonography, while simultaneously providing the functional data with regard to excretory function, renal perfusion, and blood flow (10). The most commonly used MR contrast agents are gadolinium chelates, which are filtered freely by the glomerulus without tubular secretion or reabsorption and have no known nephrotoxicity, and thus have been used as renal MRI contrast agents. Recent studies have measured relative perfusion in renal grafts by MRI following the administration of a contrast agent in an animal model (11) and in

humans (12,13). These results suggest that MR perfusion imaging of renal allografts can be used to noninvasively differentiate acute tubular necrosis from acute allograft rejection during the post-transplant period. However, using gadolinium chelates, the vascular and tubular phases are difficult to distinguish, especially at the end of the first pass, due to interstitial diffusion and elimination by glomerular filtration. Moreover, the biphasic effect is related to a weak R_2/R_1 ratio, approximately equal to 1. Thus, gadolinium chelates with dynamic MRI seem better suited for analyzing glomerular filtration than perfusion (14–16). We previously reported that a quantitative measurement of renal cortical perfusion by arterial spin-labeled MRI can provide a noninvasive diagnostic method for monitoring the status of renal transplants without using a contrast agent (17). The drawback in using the arterial spin-labeling technique in kidney is that quantitative renal cortical perfusion cannot be measured in the coronal direction due to technical constraints. Also, the left and right kidneys must be studied in separate scans since native and transplanted kidneys do not appear within the same transverse slice.

Dextran-coated ultrasmall superparamagnetic iron oxide (USPIO) particles are known to have an intravascular distribution, migrate very slowly across the capillary endothelium, and have a relatively long blood half-life (18,19). The slow elimination of these particles allows analysis of the blood pool tracer-related signal modifications, which remain stable during the observation period. The optimal dose of dextran-coated USPIO particles for a first-pass dynamic MRI study is dependent on the MR pulse sequence, field strength, etc. The purpose of the present study was to evaluate first-pass renal perfusion with different doses of dextran-coated USPIO particles in normal rats in order to find the optimal dose of USPIO particles for the chosen pulse sequence. We then applied this method to an experimental kidney transplant model in rats to evaluate whether USPIO-enhanced first-pass renal perfusion MRI can accurately detect acute renal allograft dysfunction.

In this work we also present a new signal analysis method for the automatic detection of renal rejection in kidney transplantation. Our method fits a parametric signal processing model to the intrarenal signal intensity. This parametric model is of the class of autoregressive (AR) models widely used in signal processing. The dynamics associated with the AR model closely track the dynamics of the intrarenal signal intensity. We have thus developed a metric that can be used to compare the similarity or dissimilarity of the AR models corresponding to each intrarenal signal. We show with the data collected from four isograft rats and six allograft rats that our metric is large when rejection occurs, as compared to the value of the metric when rejection does not occur.

MATERIALS AND METHODS

Animals

Inbred Dark Agouti (DA) (RT1^a) and Brown Norway (BN) (RT1^n) male rats weighing 250–300 g were purchased from Harlan-Sprague Dawley Inc. (Indianapolis, IN) and were housed in the animal facility of the Pittsburgh NMR Center for Biomedical Research. Animal care and experimenta-

tion were in compliance with the Principles of Laboratory Animal Care and Guide for the Use of Laboratory Animals, published by the National Institutes of Health (NIH Publication No. 96-03, revised 1996). The present study was approved by the Institutional Animal Care and Use Committee of Carnegie Mellon University.

Forty normal rats [DA ($N = 20$) and BN ($N = 20$)] were observed for at least 3 d before the study, and exhibited normal eating and drinking patterns. Each group was divided into four subgroups (five rats in each subgroup) receiving USPIO doses of 3.0, 6.0, 12.1, and 18.1 mg Fe/kg/body weight (or 54, 108, 216, and 324 μmol Fe/kg/body weight).

Sixteen transplanted rats underwent MR perfusion imaging of the kidneys at day 4 after transplantation. The BN rats were used as recipients throughout and as donors for syngeneic transplantation (isografts), and the DA rats served as donors for allogeneic transplantation (allografts). The animals were anesthetized by inhalation of methoxyflurane (Mallinckrodt Veterinary, Mundelein, IL). Left nephrectomy of the recipients was performed before the left kidney transplantation. The graft (the donor left kidney) was flushed with lactated Ringer's solution (Abbott Laboratories, North Chicago, IL) containing heparin and then stored in the same solution at 4°C. The ischemia time was about 25 min. Following the microsurgical technique of Lee (20), the donor renal artery and vein were anastomosed end-to-side to the recipient abdominal aorta and inferior vena cava with 10-0 sutures (Sherwood Medical, St. Louis, MO). The ureter of the recipient was anastomosed end-to-end with the donor's ureter by 10-0 sutures using four stitches. The right kidney was kept intact as an internal control for each individual transplanted rat. Six allograft (DA → BN) and four isograft (BN → BN) rats were injected with 6.0 mg Fe/kg USPIO particles, and six allograft (DA → BN) rats were injected with 12.1 mg Fe/kg USPIO particles.

Before MRI, a 30-cm PE50 extension tube was inserted into the right jugular vein for the infusion of USPIO particles. A heparinized lactated Ringer's solution was maintained in the extension tubing to prevent coagulation.

Preparation of USPIO Particles

Dextran-coated USPIO particles were synthesized in our laboratory according to Palmacci and Josephson (21) with slight modifications. A spectrophotometric method was used to determine the iron content in the particle suspensions (22). Measurements of iron-core size and mean diameter of whole particles were carried out as described in Dodd et al. (23). Iron-core size measured by transmission electron microscopy (TEM) was found to be in the range of 4.0–7.5 nm. The mean diameter of whole particles measured by laser light scattering was 27 ± 1.1 nm. The MR relaxivities, R_1 (spin-lattice relaxation rate, $1/T_1$, per mol of Fe in USPIO) and R_2 (spin-spin relaxation rate, $1/T_2$, per mol of Fe in USPIO) measured at 27.8°C with a Bruker Minispec (Bruker Canada, Ltd., Milton, Ontario, Canada) operating at 0.47 Tesla, were 3.83×10^4 and 10.8×10^4 M^{-1} s^{-1}, respectively.

For in vivo studies, the USPIO suspensions were dialyzed in phosphate-buffered saline (PBS), sterilized by filtration, and assayed for iron content (22). The solution was then diluted with PBS, and suspensions containing

3.0, 6.0, 12.1, and 18.1 mg Fe/kg were injected intravenously into the jugular vein.

Dynamic MRI Studies

All animals underwent snapshot fast low angle shot (FLASH) dynamic studies on a 4.7-T Bruker AVANCE DRX MR instrument equipped with a 40-cm horizontal bore superconducting solenoid and a 15-cm shielded gradient insert using a 7-cm diameter Bruker volume coil, which was used as an RF transmitter and receiver. MR experiments were carried out with the rats in a supine position in the center of the coil, under general anesthesia and mechanical ventilation with 2% isoflurane (Abbott Laboratories, North Chicago, IL) in an oxygen/nitrous oxide (70%:30%) mixture administered via an endotracheal intubation.

The snapshot FLASH sequence is characterized by low flip angle and very short pulse duration and signal readouts (24). This sequence consisted of a very short TE (2.1 ms) and TR (3.45 ms) with an acquisition time for a 64×38 data matrix of 134 ms per image. Because of duty cycle constraints, a time delay of 200 ms was added between successive image acquisitions. Images were thus repeated every 334 ms. The field of view (FOV) and the section thickness were 6 cm and 2 mm, respectively, and the image matrix was 64×64. Each dynamic MRI study consisted of 128 snapshot FLASH images obtained in a total imaging time of 43 s. A flip angle of approximately $\alpha = 15°$ was found to be optimal for the maximum signal intensity.

Pilot images with a T_2^*-weighted gradient-echo sequence (TR/TE = 300 ms/7 ms; Ernst angle; 128×128 matrix; 6-cm FOV) in the axial and coronal plane were initially acquired to determine the optimal coronal plane. Then, the coronal plane with 2-mm slice thickness passing through the central parts of both kidneys was chosen as the final position for the dynamic study. To confirm image quality and location, 128 dynamic snapshot FLASH images without USPIO infusion were obtained, then the extension tubing was loaded with the USPIO particles. These particles were injected simultaneously as the snapshot FLASH dynamic scan was started. All USPIO particles were bolus-injected manually, as fast as possible (<2 s), by the same operator.

Signal Intensity Analysis

Image analysis was carried out using the Bruker ParaVision software. The regional dynamics of the intrarenal signal intensity were initially studied qualitatively by visual analysis. These signal intensities were then quantified by the following procedure. For each kidney, three regions of interest (ROIs) within the cortex and three ROIs within the outer medulla were chosen. These ROIs were chosen to be the same across the 128 frames of the sequence. Each ROI was 2×2 pixels. For each frame and each kidney, the signal intensities were averaged over the three cortex ROIs across the whole sequence to obtain for each kidney one signal-intensity time series $I_c(t)$ of 128 samples. A similar procedure gave the corresponding medulla signal-intensity time series $I_m(t)$, which again had 128 samples. The

two signal intensities $I_c(t)$ and $I_m(t)$ were then normalized as a means to correct the signal changes not directly related to the USPIO particles. To achieve this normalization, across the 128 frames were first chosen the same 3×3 pixel ROI in the psoas major muscle. The psoas major muscle was selected because the muscle tissue does not take up iron (19,25). The average signal intensity $I_{psoas}(t)$ over the 9 pixels of the ROI for each frame, $t = 1,2,\ldots,128$, of the sequence was computed. Then, the two signal intensities $I_c(t)$ and $I_m(t)$ were normalized by $I_{psoas}(t)$ to obtain $S_c'(t) = I_c(t)/I_{psoas}(t)$ and $S_m'(t) = I_m(t)/I_{psoas}(t)$. Finally, the two time series were renormalized by the signal intensity obtained for the first frame in order to obtain

$$S_c(t) = S_c'(t)/S_c'(1) \qquad [1a]$$

$$S_m(t) = S_m'(t)/S_m'(1). \qquad [1b]$$

Hereafter, the subscripts in $S_c(t)$ and $S_m(t)$ are usually omitted and we simply refer to the signal intensity $S(t)$.

The ROI intensity data were then analyzed by two independent techniques. The first method involved characterizing the normalized signal intensity curve by three parameters: maximum signal decrease (MSD); time at which this MSD appeared (t_{MSD}); and wash-in slope. Standard statistical analysis of these parameters was carried out. The MSD for each dose was determined using the formula MSD = $[1 - S(t_{MSD})] \times 100\%$. The wash-in slopes of the signal intensity change were obtained by a three- to five-point linear regression on the wash-in curve ($R^2 > 0.95$). The second technique involved an autoregressive modeling and subspace distance analysis to automatically discriminate between the signals $S(t)$ corresponding to the native kidney and the signals $S(t)$ for kidneys undergoing rejection. Our method was based on an autoregressive statistical model that we fitted to the dynamic signal $S(t)$. The concept of subspace distance was used as an objective criterion for early detection of rejection.

Autoregressive Modeling

The signals are first conditioned by subtracting the sample mean $\overline{S} = \left(\frac{1}{128}\right)\sum_{t=1}^{128} S(t)$ from the original relative intensity signal $S(t)$, and then are fitted to the mean centered relative intensity signal $S(t)$ in an AR model (26). From now on, $S(t)$ is assumed as zero mean. With AR modeling, future samples of the sequence $\{S_t\}$ are modeled as a linear combination of past samples plus a noise sample $\{u_t\}$, i.e.,

$$S_t = -\sum_{i=1}^{p} a_i S_{t-i} + u_t. \qquad [2]$$

In Eq. [2], p is the AR model order and $\{a_i\}$ is the AR model coefficients (26). The sequence $\{u_t\}$ is known as the prediction error sequence. The AR model (Eq. [2]) shows that the signal sample at time t, S_t is described as a regression over the past p signal samples plus a noise u_t.

From signal processing theory, it is known that the dynamic behavior of an AR model is well characterized by its

poles (27). The poles of the AR model are the roots of the monic polynomial (the coefficient of the highest order term is 1) associated with Eq. [2]:

$$p(x) = x^p + \sum_{i=1}^{p} a_i x^{p-i}, \quad p \geq 1. \qquad [3]$$

The characteristic polynomial is of degree p, the order of the AR model, and the coefficients of the polynomial are the AR model coefficients $\{a_i\}$. We can also associate with the AR model of Eq. [2] a p-th order matrix $\mathbf{A}$ determined from the AR model coefficients $\{a_i\}$,

$$\mathbf{A} = \begin{bmatrix} 0 & 1 & \cdots & 0 \\ \vdots & \vdots & \ddots & \vdots \\ 0 & 0 & & 1 \\ -a_p & -a_{p-1} & \cdots & -a_1 \end{bmatrix}, \quad p \geq 1. \qquad [4]$$

Note that for $p = 1$, we get $\mathbf{A} = -a_1$, i.e., $\mathbf{A}$ is the scalar $-a_1$. The $\mathbf{A}$ matrix is said to be in companion form. Equation [2] can now be written in vector-matrix form by introducing the p-dimensional "state" vector as

$$\mathbf{s_t} = \begin{bmatrix} S_{t-p+1} \\ \vdots \\ \dot{S}_t \end{bmatrix}. \qquad [5]$$

We also introduce the p-dimensional unit vector as

$$\mathbf{b} = \begin{bmatrix} 0 \\ \vdots \\ 0 \\ 1 \end{bmatrix}. \qquad [6]$$

Again, if $p = 1$, then $\mathbf{b} = 1$. Equation [2] can now be rewritten as

$$\mathbf{s_{t+1}} = \mathbf{A s_t} + \mathbf{b} u_{t+1}. \qquad [7]$$

Let λ_i, $i = 1, \ldots, p$ represent the eigenvalues associated with $\mathbf{A}$, and $\boldsymbol{\omega_i}$ be the corresponding eigenvectors, i.e.,

$$\mathbf{A}\boldsymbol{\omega_i} = \lambda_i \boldsymbol{\omega_i} \quad i = 1, \ldots, p. \qquad [8]$$

All the λ_i, $i = 1, \ldots, p$ are assumed as distinct. The eigenvalues of the companion matrix $\mathbf{A}$ equal the poles of the AR model given by Eq. [2], and are also the roots of the characteristic polynomial (Eq. [3]) (26).

AR Model Fitting: Combined Information Criterion and Burg Methods

AR models are very compact statistical descriptions for the time series, i.e., instead of working with the 128 samples of the time series, we only need to work with the p AR model coefficients $\{a_i\}$. This may represent considerable data reduction. The challenge is to determine the order p and the AR coefficients $\{a_i\}$ of the AR model. The combined information criterion (CIC) (28) is used to select the order of the AR model. The CIC is defined as

$$\text{CIC}(p) = \ln\{\text{RES}(p)\} + \max\left[\prod_{i=0}^{p} \frac{(1 + v_i)}{(1 - v_i)} - 1, 3 \sum_{i=0}^{p} v_i \right], \qquad [9]$$

where ln is the natural logarithm, Π stands for the product (multiplication), max returns the max of the two quantities in its argument, and RES(p), is the residue noise variance

$$\text{RES}(p) = \frac{1}{N - p} \sum_{t=p+1}^{N} [S_t - (-\sum_{i=1}^{p} a_i S_{t-i})]^2, \qquad [10]$$

and the $\{v_i\}$ are referred to as the finite sample variance coefficients (28).

There are several possible choices for the coefficients $\{v_i\}$ in Eq. [9] corresponding to different possible methods to estimate the AR coefficients $\{a_i\}$. We have chosen to estimate the AR coefficients by application of Burg's method (29) (for details, see Appendix A). Burg's method is based on the minimization of the sum of the forward and backward squared prediction errors. Accordingly, we have chosen

$$v_{i,Burg} = \frac{1}{(N + 1 - i)}. \qquad [11]$$

The order p selected for the AR model is referred to as M, which is given by

$$M = \arg\min_{p} (\text{CIC}(p)), \qquad [12]$$

i.e., it is the value of p such that the quantity CIC(p) in Eq. [9] is minimized.

By applying CIC(p) to the test data presented below, we have found that a fourth-order AR model represents the best fit for the several relative intensity signals under study. From the estimates $\{\hat{a}_i\}$ of the AR coefficients found with Burg's method, we have determined the poles of the AR model by rooting the polynomial in Eq. [3]. As noted above, the poles are the eigenvalues $\{\hat{\lambda}_i\}$ of the companion matrix $\mathbf{A}$. The associated eigenvectors $\{\hat{\omega}_i\}$ have also been determined. As shown in the next section, the poles of the AR model corresponding to the transplanted kidney, and the poles of the AR model corresponding to the native kidney may exhibit different patterns. The poles may be complex numbers. We consider next how to best quantify the similarity or dissimilarity between these two sets of poles corresponding to the native and transplanted kidneys.

Subspace Distance

The Euclidean distance between the set of poles is not a good measure for pattern similarity. We propose, instead, to measure the similarity or dissimilarity between the pole configurations by a subspace distance. This provides us with a quantitative criterion for decision-making. The subspaces of interest are the subspaces spanned, or generated, by the eigenvectors (modes of the AR model). Since $\mathbf{A}$ is 4×4, if we use the corresponding four eigenvectors, a 4D space is obtained. Using all four eigenvectors gives the
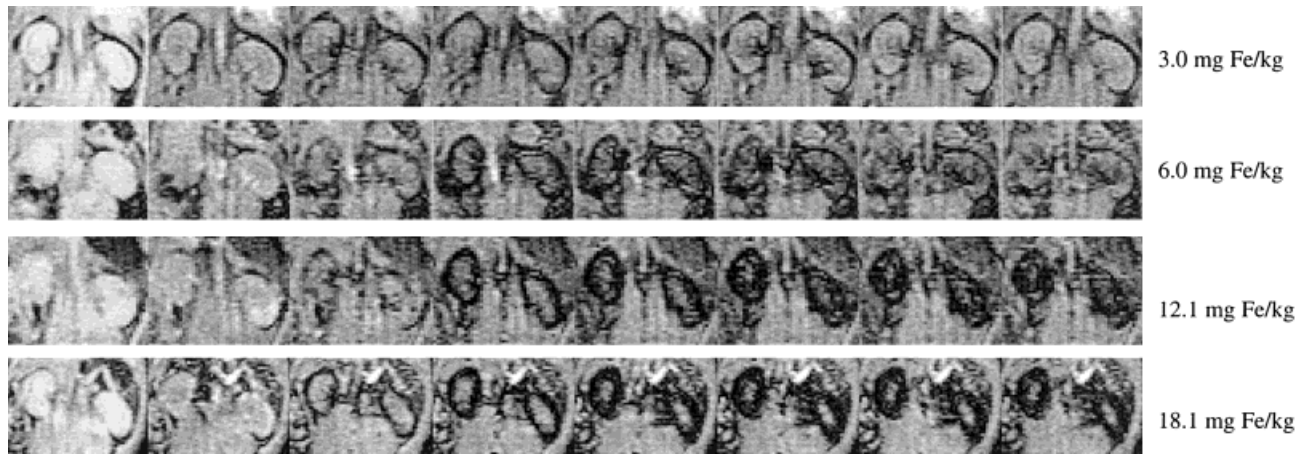
FIG. 1. Representative dynamic snapshot FLASH MR images at selected time points with four different USPIO doses in normal BN rats. Shown from left to right are images at time periods of 0, 2.4, 4.4, 6.4, 8.4, 10.4, 12.4, and 14.4 s after USPIO infusion.

whole space, so there is no distinction between the space corresponding to the left and right kidneys. Hence, we need to use a subcollection of the four eigenvectors. In Fig. 2a and b, the four star poles and the four diamond poles are grouped into two pairs: the left pair (poles roughly at the $[-0.5, \pm 0.5]$ positions) and the right pair (close to the [0,1] position). Focusing on the left pair of poles, it is seen that, in plots a and b, the diamonds are close to the stars. On the other hand, with the right pair of poles, the diamonds are close to the stars on plot a, while the diamonds have moved to the real line (horizontal axis) on plot b. Because of this dissimilarity in the pattern of the right pair of poles, we have chosen to work with the subspaces spanned by the two eigenvectors associated with the right pair of poles. For each of the left and right kidneys, we superscript these eigenvectors $\hat{\omega}_i$, $i = 1, 2$, by L and R to indicate the left and right kidneys, respectively.

We consider the subspace spanned, i. e., generated, by the pair of eigenvalues associated with the left kidney, $\hat{\omega}_i^L$, $i = 1,2$, and the subspace spanned by the pair $\hat{\omega}_i^R$, $i = 1,2$, associated with the right kidney. A distance between these two subspaces is introduced. To do that, the 4×2 matrices are defined as

$$\mathbf{V_L} = [\; \hat{\omega}_1^L \quad \hat{\omega}_2^L \;] \qquad [13a]$$

$$\mathbf{V_R} = [\; \hat{\omega}_1^R \quad \hat{\omega}_2^R \;]. \qquad [13b]$$

The distance between the subspaces that quantifies the dissimilarity between the left and right kidneys is calculated by

$$D = \|\mathbf{V_L}(\mathbf{V_L}^H\mathbf{V_L})^{-1}\mathbf{V_L}^H - \mathbf{V_R}(\mathbf{V_R}^H\mathbf{V_R})^{-1}\mathbf{V_R}^H\|_2, \qquad [14]$$

where $\mathbf{V}_L^H$ is the transpose conjugate of the matrix $\mathbf{V_L}$, and $\|B\|_2$ is the spectral norm of the matrix B computed by

$$\|\mathbf{B}\|_2 = \sqrt{\lambda_{\max}} \qquad [15]$$

with $\lambda_{\max}$ the maximum eigenvalue of $\mathbf{B}^T\mathbf{B}$ (30). Note that the subspace distance is bounded, i.e., $0 \le D \le 1$ (see Ref.

30). Note that in Eq. [14], $\mathbf{V_L}$ is 4×2 and noninvertible, but $\mathbf{V_L}\,^H\mathbf{V_L}$ is 2×2 and invertible. A similar condition holds for $\mathbf{V_R}$.

Histopathology

All transplanted rats were sacrificed after the MRI examinations, and the kidneys were removed for evaluating the pathological changes. Kidneys were cut in the same coronal orientation as the section orientation of the MR images. The samples were fixed in 4% paraformaldehyde, embedded in paraffin, and processed for 5-μm sections. Hematoxylin-eosin (H & E) staining was performed in the Transplantation Pathology Laboratory of the University of Pittsburgh Medical Center.

Statistical Analysis

For statistical analysis, differences among the four doses in normal rats were examined by Kruskal-Wallis analysis, and differences between the left and right kidneys with respect to MSD, t_{MSD}, and wash-in slope were analyzed
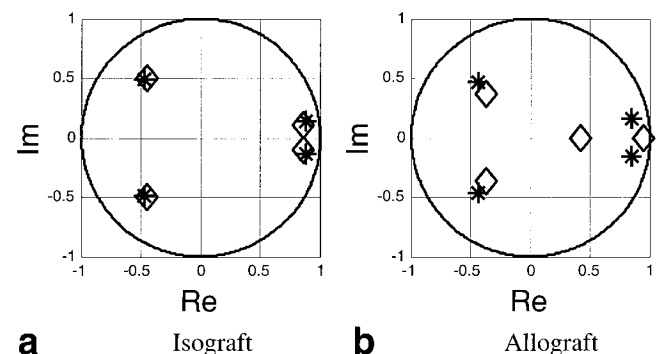

FIG. 2. The poles of the AR model of the signal in the cortex for two rats: (**a**) isograft and (**b**) allograft. The stars represent the poles of the right kidney, and the diamonds represent the poles of the left kidney. Im = imaginary part; Re = real part; ✳ = native kidney; and ◇ = transplanted kidney.
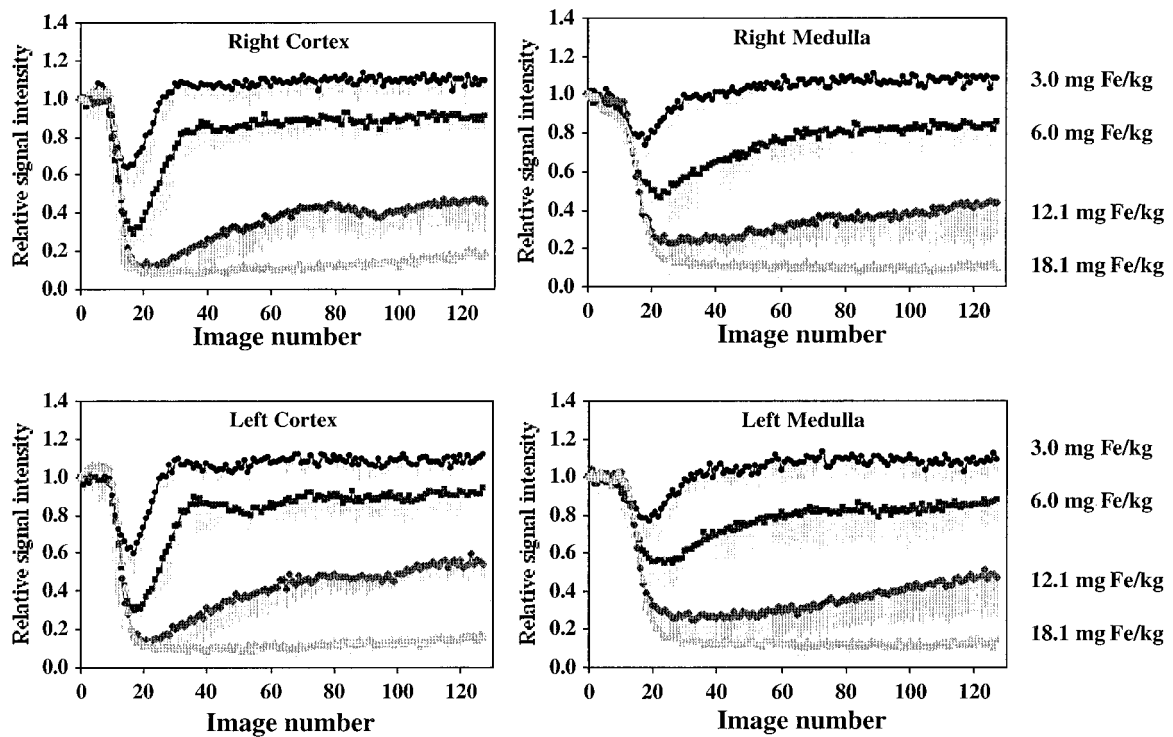
FIG. 3. Plots of the relative signal intensity changes vs. time in the cortex and the outer medulla in normal BN rats after a bolus injection of four different doses. Images were repeated at 334 ms. Shaded bars represent the SDs of the normalized signal intensities.

with the paired *t*-test. A probability level (P) < 0.01 was considered significant.

RESULTS

Normal Rats

Because the optimal dose is related to the MR pulse sequence selected, we have evaluated first-pass renal perfusion with different doses of USPIO particles in normal rats in order to find the optimal dose of USPIO particles for the chosen pulse sequence. Our previous study (31) showed that the allograft (DA → BN) undergoes moderate acute rejection on day 4 after transplantation. We chose day 4 post-transplantation as the time point for the first-pass dynamic study. All animals survived after bolus USPIO infusion. All kidneys with the doses of 3.0, 6.0, and 12.1 mg Fe/kg showed signal intensity changes typical of first-pass transit of a bolus of USPIO particles through the kidney vasculature. Figure 1 shows MR images at selected time points following bolus injection of USPIO particles of 3.0, 6.0, 12.1, and 18.1 mg Fe/kg, respectively. We observed a signal intensity decrease within the cortex first, followed by a centripetal progression of the signal decrease toward the medulla. This was followed by a signal intensity increase in the cortex and the medulla because of the wash-out of the bolus. In the kidneys with a dose of 18.1 mg Fe/kg, no increase of the signal intensity was observed after the initial signal intensity decrease in the cortex and the outer medulla. The plots for the regional change in the relative signal intensity over time in the BN rats are presented in Fig. 3. Data points represent the means of the normalized regional signal intensities $S(t)$ for

all rats in the group; shaded bars represent the standard deviation (SD) of this mean. Well-shaped first-pass dynamic curves are demonstrated only for the doses of 3.0 and 6.0 mg Fe/kg in the cortex. The dynamic curve appears more rounded at the dose of 12.1 mg Fe/kg. With the dose of 18.1 mg Fe/kg, the dynamic curve does not recover after maximum signal intensity reduction. A steep decrease of relative signal intensity in the cortex and a gradual decrease of relative signal intensity in the outer medulla have been observed at all doses. This signal intensity change is symmetric; no significant differences for MSD, t_{MSD}, or wash-in slope are observed between the right and the left kidneys at all four doses. Table 1 summarizes the means of MSD, t_{MSD}, and wash-in slope for the renal cortex of all rats studied in the various groups. Higher MSD, t_{MSD}, and wash-in slope appear with higher doses of USPIO particles. However, the MSD, t_{MSD}, and wash-in slope at 12.1 and 18.1 mg Fe/kg are not significantly different in the cortex. The dynamic curves in DA rats show shapes similar to those observed in the BN rats. However, as shown in Table 1, with the same USPIO dose, lower MSD, shorter t_{MSD}, and higher wash-in slope values in the cortex are observed in the DA rat group ($P < 0.01$). With the 12.1 mg Fe/kg USPIO dose, the dynamic curve in the DA rats appears to recover faster than that in the BN rats.

Rats With Transplanted Kidneys

All animals survived after infusion of a bolus of USPIO containing 6.0 or 12.1 mg Fe/kg. The allograft kidneys show graft enlargement and a delayed perfusion pattern compared with normal kidneys. Isografts show perfusion

Table 1
MSD Values, Time of Occurrence of MSD, and Wash-In Slope in the Cortex Following Infusion of USPIO Particles

	MSD (%)		t_{MSD} (s)		Slope (per s $\times 10^{-2}$)	
	Right	Left	Right	Left	Right	Left
BN rats						
3.0 mg Fe/kg (N = 5)	38.4 ± 7.4	41.4 ± 6.2	5.1 ± 0.4	5.1 ± 0.3	−3.0 ± 0.4	−3.4 ± 0.4
6.0 mg Fe/kg (N = 5)	76.8 ± 6.5	74.1 ± 1.5	6.0 ± 0.9	6.2 ± 0.7	−5.5 ± 0.5	−5.6 ± 0.7
12.1 mg Fe/kg (N = 5)	89.8 ± 1.4	87.8 ± 1.5	6.8 ± 0.8	6.6 ± 0.5	−6.9 ± 0.8	−7.2 ± 1.2
18.1 mg Fe/kg (N = 5)	92.0 ± 4.2	91.2 ± 3.2	7.3 ± 0.4	7.1 ± 0.7	−6.9 ± 0.9	−6.8 ± 0.8
DA rats						
3.0 mg Fe/kg (N = 5)	30.2 ± 7.5	26.9 ± 10.2	3.1 ± 0.4	3.0 ± 0.4	−4.1 ± 1.2	−4.4 ± 1.1
6.0 mg Fe/kg (N = 5)	61.0 ± 6.0	60.8 ± 11.6	3.4 ± 0.5	3.7 ± 0.3	−7.7 ± 1.6	−7.6 ± 1.7
12.1 mg Fe/kg (N = 5)	84.9 ± 4.6	85.8 ± 3.3	4.4 ± 0.4	4.3 ± 0.3	−8.2 ± 1.1	−8.1 ± 1.5
18.1 mg Fe/kg (N = 5)	90.0 ± 2.3	90.8 ± 1.3	5.0 ± 0.5	5.0 ± 0.6	238.2 ± 2.7	−8.1 ± 2.5
Allograft (DA → BN)						
6.0 mg Fe/kg (N = 6)	78.3 ± 5.5	55.8 ± 9.4[a]	5.3 ± 1.2	6.7 ± 1.1[a]	−5.5 ± 0.8	−2.7 ± 1.3[a]
12.1 Fe/kg (N = 6)	88.2 ± 3.5	72.1 ± 11.4[a]	5.6 ± 0.6	7.2 ± 0.8[a]	−6.7 ± 0.8	−4.4 ± 1.3[a]
Isograft (BN → BN)						
6.0 mg Fe/kg (N = 4)	78.1 ± 6.9	75.9 ± 9.3	5.3 ± 0.5	5.7 ± 1.4	−5.4 ± 1.4	−4.7 ± 1.0

All values are expressed as mean ± SD. MSD, maximal signal decrease; t_{MSD}, time of maximal signal decrease.
[a]$P < 0.01$ versus contralateral kidney. In the rats with transplanted kidneys, the right kidney is native; the left kidney is the graft.

patterns similar to those of normal kidneys. The plots for regional changes in the relative signal intensity over time in the transplanted rats are presented in Fig. 4. Well-shaped first-pass dynamic curves are demonstrated for doses of both 6.0 and 12.1 mg Fe/kg in the cortex in native kidney (right kidney). Allograft kidneys (left kidney) show lower MSD, delayed t_{MSD}, and lower wash-in slope compared with normal kidneys (all $P < 0.01$) (Table 1). A greater decrease of signal intensity in the cortex and me-

dulla is observed with increasing dose of USPIO particles. The perfusion patterns in the cortex and outer medulla of the isograft kidneys are similar to those of normal kidneys (Fig. 5). No significant differences for the MSD, t_{MSD}, or wash-in slope are observed between the native kidney (right kidney) and the isograft kidney (left kidney).

The primary goal of this study is to develop a technique to detect organ rejection via MR-observable indices. It appears that all three parameters characterizing the MR
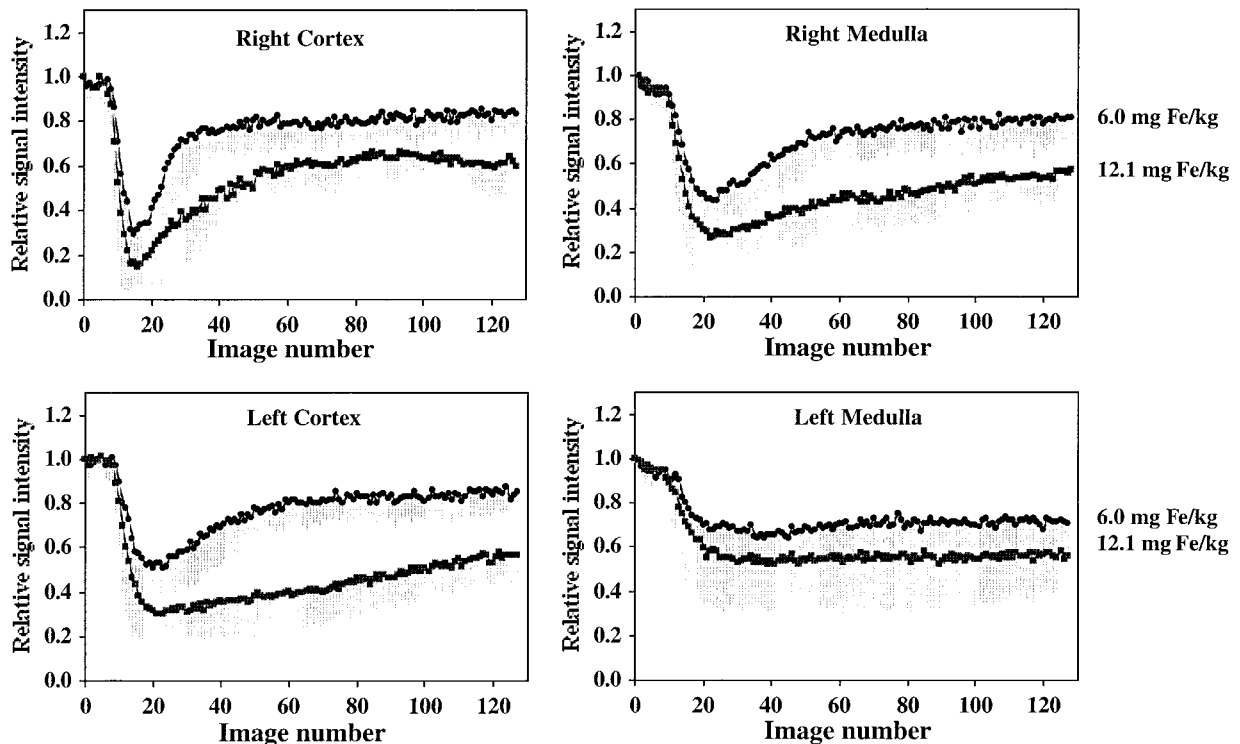

FIG. 4. Plots of the relative signal intensity changes vs. time in the cortex and the outer medulla in the allograft rats after a bolus injection of two different doses. Images were repeated at 334 ms. Shaded bars represent the SDs of the normalized signal intensities.
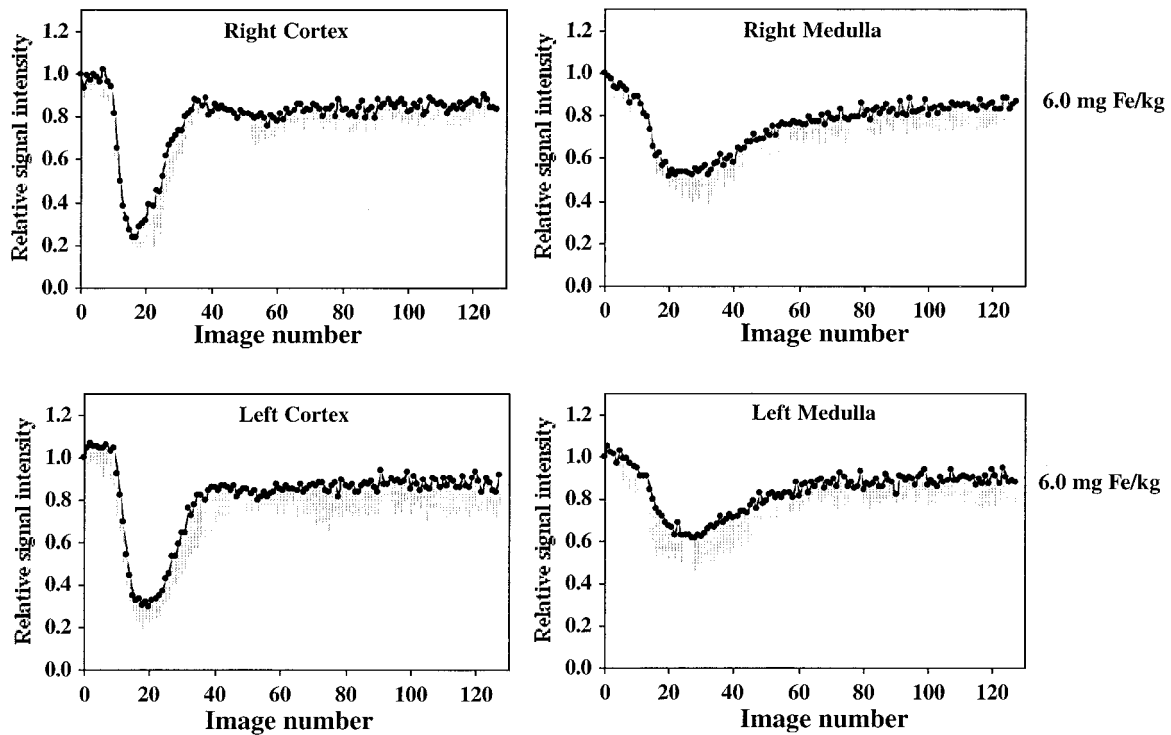
FIG. 5. Plots of the relative signal intensity changes vs. time in the cortex and the outer medulla in the isograft rats after a bolus injection of 6.0 mg Fe/kg. Images were repeated at 334 ms. Shaded bars represent the SDs of the normalized signal intensities.

signal during wash-in/wash-out of the USPIO bolus, i.e., MSD, t_{MSD}, and wash-in slope, of the allografts are different from those of the isografts and the native kidneys, and thus may be used as indices of organ rejection. While each of these parameters shows differences in the allografts compared to the isografts and the native kidneys, these parameters considered as a set will show wider differences between normal and diseased kidneys. To define a range for these sets of parameters for normal and transplanted kidneys, we have created scatter plots using the individual data for all rats. A scatter plot of all three parameters for normal kidneys will yield a 3D plot from which a range of normal values can be identified. For illustrative purposes, we present in Fig. 6 a 2D scatter plot for t_{MSD} vs. MSD, which shows enhanced differences between normal and diseased kidneys when the parameter pairs are considered together. It is apparent that the t_{MSD}/MSD parameter pairs for kidneys with normal function cluster around the dotted area, which can be regarded as the range of normal values. Values outside this region are considered abnormal, with rejecting kidneys characterized by a shift of the parameter pair upwards and to the left. Another method of incorporating the combined effect of MSD, t_{MSD}, and wash-in slope is (as described above) through autoregressive modeling and subspace analysis, in which a single parameter, the subspace distance, characterizes the difference in the shape of the wash-in/wash-out curves between a normal and a diseased kidney.

We have applied the AR model fitting technique by fitting an AR model to each of the relative intensity signals $S(t)$ under study. We present here only the results for the cortex relative intensity signals for the left and right kid-

neys, for each of the six allograft rats, and for each of the four isograft rats after USPIO infusion of a dose of 6.0 mg Fe/kg USPIO. We have repeated these studies with the medulla signals for both groups of rats, but have found that the cortex signals provide better discrimination for early rejection detection. In the present study, we present only the results for the cortex signals.

Figure 2 displays, on the complex plane, the configuration of the resulting poles (eigenvalues) of the AR model for each of four cases: (i) the left kidney cortex signal (transplanted kidney, $\diamond$), (ii) the right kidney cortex signal (native kidney, $\ast$), (iii) for one of the isograft rats (left plot), and (iv) one of the allograft rats (right plot).

We now interpret these complex plane pole configurations of the AR model. First, note that for each cortex signal, the four poles come into two pairs; for example, the four diamonds on the left plot can be grouped into a pair of diamonds on the left of the plot (left pair) and a pair of diamonds on the right of the plot (right pair). Similarly, the diamonds on the right plot can be grouped into two pairs, as can the four stars in each of the plots. As shown in Fig. 2, it is apparent that in the isograft case the poles of the left and the right kidneys are quite close to each other. In other words, the left and right pairs of diamond and star poles are very close to each other on the left plot of Fig. 2, and these poles display a very similar pattern. In contrast, in the allograft cases the pattern for the right pair of poles of the transplanted kidney is quite different from the pattern of the right pair of poles of the native kidney. This pattern of similarity and dissimilarity among the left and right pairs of poles was systematically observed in all four isograft rats and six allograft rats studied. We used the
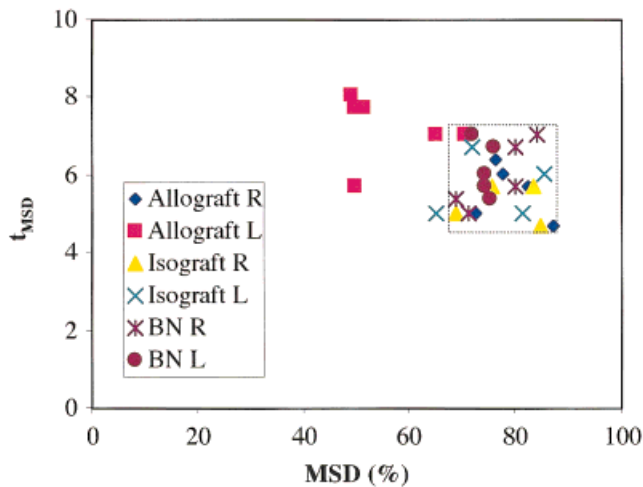
FIG. 6. Plot for t_{MSD} vs. MSD shows enhanced differences between normal and transplanted kidneys when the parameter pairs are considered together. It is apparent that the t_{MSD}/MSD parameter pair for the kidneys with normal function clusters around the area bounded by the dotted area, which can be regarded as the range of normal values.

pattern for the right pair of poles as the distinguishing characteristic between the healthy kidney and transplanted kidneys undergoing rejection.

We computed the subspace distance given by Eq. [14] for the subspaces associated with the right pair of poles for the AR models fitting the data $\{S_t\}$ for each individual rat in the two groups of allograft and isograft rats. Figure 7 shows a bar diagram for the subspace distances of the cortex signals between the left and right kidneys for each of the four isograft rats and each of the six allograft rats. From Fig. 7, we conclude that the subspace distances for the cortex signals between the left and right kidneys for the six allograft rats are consistently larger than the distances for the four isograft rats. The mean ± SD of these subspace distances is 0.1926 ± 0.1459 for the allograft rats vs. 0.0227 ± 0.0066 for the isograft rats. These results are consistent with those obtained with the Kruskal-Wallis analysis in terms of the MSD, t_{MSD}, and the wash-in slope. It is reasonable to infer that the subspace distance between the left and right kidneys is a good measure for investigating kidney function dissimilarity.

Histopathology of kidneys at four days after transplantation shows early acute rejection in all allografts, which is characterized by graft enlargement; entire interstitial infiltration by mononuclear inflammatory cells, particularly in or around glomeruli and the perivascular area; foci of moderate or severe tubulitis; and mild intimal arteritis (Fig. 8a and b). All isografts show normal kidney architecture and some tubular edema is observed in isografts, but without damage to the renal parenchyma and vessels (Fig. 8c and d).

DISCUSSION

The diagnostic accuracy of renal perfusion MRI can be improved by using a contrast agent that would only study perfusion and would have no interstitial diffusion, glomer-

ular filtration, or tubular excretion. Dextran-coated iron oxide particles are such a type of blood pool agent, and have a safety margin considerably higher than that of conventional radiopaque and paramagnetic MR contrast agents (25). Because of the local field inhomogeneity induced by the susceptibility effects of iron oxide particles within and around the vessels, decreased signal intensity within the renal parenchyma is linked mostly to spin dephasing. Thus, the MRI potential of dextran-coated superparamagnetic iron oxide (SPIO) and USPIO has been the focus of many investigations (18,19,32–34).

SPIO particles (30–1000 nm in diameter) are useful as renal perfusion MRI markers in organs during the initial postinjection period (32). SPIO particles have the advantage of increased relaxivity and high magnetic susceptibility (33). The susceptibility allows for first-pass MRI with high signal loss after administration of a small volume in a narrow bolus. Thus, SPIO particles can act as an MRI superparamagnetic negative blood-pool contrast agent, which can be used to mark the vascular compartment. Trillaud et al. (34) carried out a first-pass study of renal perfusion in the rabbit using SPIO with turbo FLASH MRI, and showed the effectiveness of SPIO in the qualitative evaluation of first-pass renal perfusion. However, the turbo FLASH sequence they used allowed a temporal resolution of approximately 1 s. This coarse temporal resolution probably explains why not much difference was observed in the first-pass dynamic curves between the cortex and the outer medulla. Furthermore, using SPIO particles has the drawback that the rapid uptake by the mononuclear phagocytic system (MPS) precludes steady-state examination of the vascular sector of kidney. The smaller USPIO particles (<30 nm in diameter) have an intravascular distribution, migrate very slowly across the capillary endothelium, and have a blood half-life of 81 min in rats (19). The slow elimination of these particles allows analysis of the tracer-related signal modifications, which remain stable during the observation period. Therefore, the prolonged blood pool effect of USPIO particles, compared with SPIO, indicates their potential utility for assessing vascular structure (18).
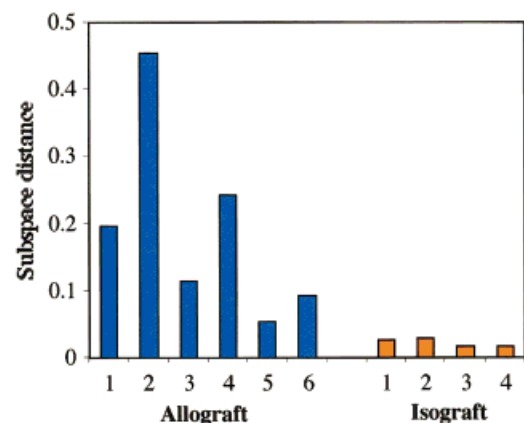

FIG. 7. The subspace distances between the left and right kidneys for six allograft and four isograft rats. The left six columns represent the allograft rats, and the right four columns represent the isograft rats.
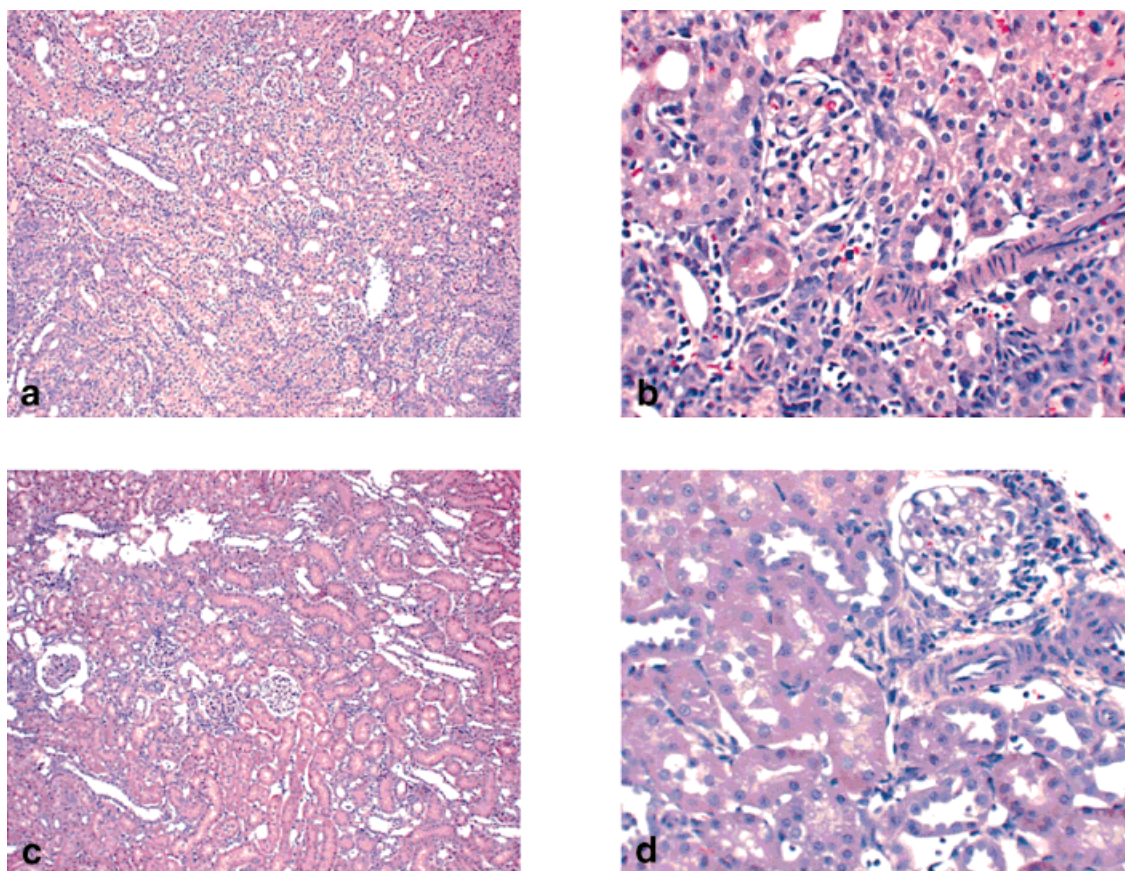
FIG. 8. Hematoxylin and eosin staining of kidney grafts on day 4 post-transplantation at (**a** and **c**) 100× and (**b** and **d**) 400× magnification. **a** and **b:** Allografts exhibit a significant amount of mononuclear cell infiltration, interstitial edema, and tubulitis. **c** and **d:** Isografts exhibit normal kidney architecture with mild focal interstitial mononuclear cell infiltration and slight tissue edema.

The evaluation of renal perfusion with MRI has become feasible with the development of rapid data acquisition techniques, which allow collection of an image in less than 1 s. Signal vs. time following injection of contrast agents could be plotted pixel-by-pixel to characterize and evaluate regional perfusion (14). We designed the renal perfusion study in normal rats to use a snapshot FLASH sequence, which allows acquisition times of 134 ms for an image (Fig. 1). We used a bolus tracking method to evaluate local renal blood flow with different doses of USPIO particles. It is clear from our data that first-passage of bolus through the kidneys is completed in less than 10 s. Accurate measurement of the time course of this passage is needed to obtain reliable values of t_{MSD}, wash-in/wash-out slope, etc. This can be achieved only with very high temporal resolution. To our knowledge, this work has the fastest acquisition time used to date for evaluating first-pass renal perfusion.

The TR in the snapshot FLASH sequence may be too short to allow for complete dephasing of the spins in the transverse plane. After the first several cycles, the residual transverse magnetization gradually reaches a steady state. For this reason, we used the signal intensities of the muscle to rectify those of the cortex and outer medulla. Using this fast gradient-echo sequence, first-pass dynamic curves

were clearly detected with doses of 3.0 and 6.0 mg Fe/kg USPIO particles. Based on the data of maximal signal reduction and wash-in, we found 6.0 mg Fe/kg USPIO particles to be a good dose for evaluating renal blood status in normal rats.

The kidney, which is the most important organ for maintaining ion/electrolyte homeostasis, are composed of two major regions: the cortex and the medulla. Glomerular filtration and proximal tubular resorption take place in the cortex, which has a very high blood flow (approximately 85% of the total renal blood flow), while the medulla participates in urine concentration-dilution phenomena and has a lower blood flow (15% of the total renal blood flow). In the present study, the differences in the plots of signal intensity vs. time in the cortex and outer medulla probably reflect differences in blood flow in each compartment. Our dynamic curves show that the transit and wash-out of the USPIO particles are rapid in the cortex. In the outer medulla, where blood flow is not as high, transit appears to be slower and wash-out appears to occur later. The results for the normal rats were used as a standard in our extended study to evaluate renal perfusion status in rats with transplanted kidneys.

Some recent reports indicate that MR perfusion imaging using gadolinium chelates could be useful to differentiate

acute tubular necrosis from acute allograft rejection during the post-transplant period in patients (12,13,35). Although the first-pass dynamic curves from gadolinium chelates were not so well defined as those obtained from our USPIO study, gadolinium-enhanced dynamic MRI still seems to be a helpful diagnostic technique for the noninvasive evaluation of graft status in patients with renal allograft dysfunction during the post-transplant period. In another study, Beckmann et al. (11) used superparamagnetic contrast agent nanoparticles coated with bovine serum albumin as an MR contrast agent to evaluate transplant models in rats. Orthotopic DA → Lewis rat kidney allografts were analyzed by T_1- and T_2-weighted spin-echo images and bolus-tracking perfusion assessment. MRI anatomical scores (range 1–6) and perfusion rates were compared with graft histology (range of rejection score 1–6). Their study showed that MRI scores correlated significantly with the histological scores, and perfusion rates correlated significantly with the MRI score or the histological score in both the acute and chronic phases of rejection. The utility of MRI with the use of USPIO particles to demonstrate renal nephrotoxicity has been reported in other recent studies (36,37). However, to our knowledge, dextran-coated USPIO particles have not previously been used to study renal perfusion in transplantation. In the experimental design of this study, acute allograft rejection was induced in BN rat recipients of a DA kidney. Acute allograft rejection could be differentiated from normal native and isograft kidney on day 4 after transplantation. Our results demonstrate that first-pass USPIO-enhanced dynamic curves sensitively reflect histopathologic changes in the early stage of acute renal rejection.

We propose calculation of a subspace distance to measure the similarity between the intrarenal relative intensity signals of the normal kidney and the transplanted kidney in rats. The subspace distance captures the dynamic behavior of the relative intensity signal (for example, MSD, t_{MSD}, and wash-in slope) in a single quantitative measure. It is a good measure with which to compare kidney functionality patterns. We have tested this quantitative criterion on four isograft and six allograft rats after a bolus USPIO infusion of a dose of 6.0 mg Fe/kg. The results demonstrate that the subspace distance can detect pattern dissimilarity in dynamic intrarenal signals, and can be a candidate for clinical assessment of kidney function.

In conclusion, this study demonstrates that rapid dynamic MRI with bolus administration of different doses of USPIO yields a reproducible first-pass perfusion pattern of USPIO particles in the kidney. The use of USPIO particles as blood pool agents with a high temporal resolution sequence appears to be an excellent way to evaluate renal perfusion. A dose of 6.0 mg Fe/kg appears to be optimal for maximal signal reduction and fast wash-out in rat kidneys. Our results clearly show a good agreement between renal graft perfusion and histopathological changes associated with rejection. The statistical model and distance criterion used in this work provide a quantitative means to evaluate kidney function. Thus, our USPIO-enhanced dynamic MRI methodology may provide a useful noninvasive tool to evaluate acute allograft rejection.

APPENDIX A

CIC(p) is computed from Eq. [9] successively for several values of the order of the AR model, $p = 1,2,\ldots P$. For each p, CIC(p) has two terms. The first term requires knowledge of the AR coefficients. We collect in this Appendix the equations for Burg's method to estimate the AR coefficients $\{a_i\}$ when the order p of the AR model is fixed. These equations can be found, for example, in Ref. 30. In the sequel, N is the number of samples; in our experiments, $N = 128$. Also, * stands for complex conjugate. Because in our case the data are real valued, * can be ignored. Burg's method for estimation of the AR coefficients is given by the following set of equations. Note that these equations are used for each value of $p = 1,2,\ldots P$. Initialization:

$$\hat{r}_{SS}[0] = \frac{1}{N}\sum_{t=1}^{N}|S(t)|^2$$

$$\hat{\rho}_0 = \hat{r}_{SS}[0]$$

$$\hat{e}_0^f[t] = S[t] \quad t = 2, 3, \ldots, N$$

$$\hat{e}_0^b[t] = S[t] \quad t = 1, 2, \ldots, N-1.$$

Iteration:

For $k = 1, 2 \ldots, p,$

$$\hat{k}_k = \frac{-2\sum_{t=k+1}^{N}\hat{e}_{k-1}^f[t]\hat{e}_{k-1}^b[t-1]^\star}{\sum_{t=k+1}^{N}(|\hat{e}_{k-1}^f[t]|^2 + |\hat{e}_{k-1}^b[t-1]|^2)}$$

$$\hat{\rho}_k = (1 - |\hat{k}_k|^2)\hat{\rho}_{k-1}$$

$$\hat{a}_k[i] = \begin{cases} \hat{a}_{k-1}[i] + \hat{k}_k\hat{a}_{k-1}^\star[k-i] & \text{for } i = 1, 2, \ldots, k-1 \\ \hat{k}_k & \text{for } i = k. \end{cases}$$

(If $k = 1$, $\hat{a}_1[1] = \hat{k}_1$.)

$$\hat{e}_k^f[t] = \hat{e}_{k-1}^f[t] + \hat{k}_k\hat{e}_{k-1}^b[t-1]$$
$$t = k+2, k+3, \ldots, N$$

$$\hat{e}_k^b[t] = \hat{e}_{k-1}^b[t-1] + \hat{k}_k^\star\hat{e}_{k-1}^f[t]$$
$$t = k+1, k+2, \ldots, N-1.$$

The estimates are given as $\{\hat{a}_p[1], \hat{a}_p[2], \ldots, \hat{a}_p[p], \hat{\rho}_p\}$. Note that in our notation

$$\hat{a}_1 = \hat{a}_p[1], \; \hat{a}_2 = \hat{a}_p[2], \ldots, \hat{a}_p = \hat{a}_p[p].$$

REFERENCES

1. U.S. Department of Health and Human Services. Annual report of the U.S. scientific registry of transplant recipients and the organ procurement and transplantation network: transplant data: 1990–1999. Public Health Services, Bureau of Health Resources Department, Division of Organ Transplantation, Bethesda, MD; UNOS, Richmond, VA; 2000.

2. Rigg KM. Renal transplantation: current status, complications and prevention. J Antimicrob Chemother 1995;36 Suppl:B51–B57.

3. Helenon O, Attlan E, Legendre C, Hanna S, Denys A, Souissi M, Kreis H, Moreau JF. Gd-DOTA-enhanced MR imaging and color Doppler US of renal allograft necrosis. Radiographics 1992;12:21–33.

4. Grenier N, Douws C, Morel D, Ferriere JM, Le Guillou M, Potaux L, Broussin J. Detection of vascular complications in renal allografts with color Doppler flow imaging. Radiology 1991;178:217–223.

5. Hanna S, Helenon O, Legendre C, Chiche JF, Di Stefano D, Kreis H, Moreau JF. MR imaging of renal transplant rejection. Acta Radiol 1991;32:42–46.

6. Hricak H, Terrier F, Demas BE. Renal allografts: evaluation by MR imaging. Radiology 1986;159:435–441.

7. Rholl KS, Lee JK, Ling D, Sicard GA, Griffith RC, Freeman M. Acute renal rejection versus acute tubular necrosis in a canine model: MR evaluation. Radiology 1986;160:113–117.

8. Liou JT, Lee JK, Heiken JP, Totty WG, Molina PL, Flye WM. Renal transplants: can acute rejection and acute tubular necrosis be differentiated with MR imaging? Radiology 1991;179:61–65.

9. Winsett MZ, Amparo EG, Fawcett HD, Kumar R, Johnson Jr RF, Bedi DG, Winsett OE. Renal transplant dysfunction: MR evaluation. Am J Roentgenol 1988;150:319–323.

10. Krestin GP. Magnetic resonance imaging of the kidneys: current status. Magn Reson Q 1994;10:2–21.

11. Beckmann N, Joergensen J, Bruttel K, Rudin M, Schuurman HJ. Magnetic resonance imaging for the evaluation of rejection of a kidney allograft in the rat. Transpl Int 1996;9:175–183.

12. Preidler KW, Szolar D, Schreyer H, Ebner F, Kern R, Holzer H, Horina JH. Differentiation of delayed kidney graft function with gadolinium-DTPA-enhanced magnetic resonance imaging and Doppler ultrasound. Invest Radiol 1996;31:364–371.

13. Szolar DH, Preidler K, Ebner F, Kammerhuber F, Horn S, Ratschek M, Ranner G, Petritsch P, Horina JH. Functional magnetic resonance imaging of human renal allografts during the post-transplant period: preliminary observations. Magn Reson Imaging 1997;15:727–735.

14. Carvlin MJ, Arger PH, Kundel HL, Axel L, Dougherty L, Kassab EA, Moore B. Use of Gd-DTPA and fast gradient-echo and spin-echo MR imaging to demonstrate renal function in the rabbit. Radiology 1989;170:705–711.

15. Choyke PL, Frank JA, Girton ME, Inscoe SW, Carvlin MJ, Black JL, Austin HA, Dwyer AJ. Dynamic Gd-DTPA-enhanced MR imaging of the kidney: experimental results. Radiology 1989;170:713–720.

16. Kikinis R, von Schulthess GK, Jager P, Durr R, Bino M, Kuoni W, Kubler O. Normal and hydronephrotic kidney: evaluation of renal function with contrast-enhanced MR imaging. Radiology 1987;165:837–842.

17. Wang JJ, Hendrich KS, Jackson EK, Ildstad ST, Williams DS, Ho C. Perfusion quantitation in transplanted rat kidney by MRI with arterial spin labeling. Kidney Int 1998;53:1783–1791.

18. Trillaud H, Degreze P, Combe C, Palussiere J, Chambon C, Grenier N. Evaluation of intrarenal distribution of ultrasmall superparamagnetic iron oxide particles by magnetic resonance imaging and modification by furosemide and water restriction. Invest Radiol 1994;29:540–546.

19. Weissleder R, Elizondo G, Wittenberg J, Rabito CA, Bengele HH, Josephson L. Ultrasmall superparamagnetic iron oxide: characterization of a new class of contrast agents for MR imaging. Radiology 1990;175:489–493.

20. Lee S. An improved technique of renal transplantation in the rat. Surgery 1967;61:771–773.

21. Palmacci S, Josephson L. Synthesis of polysaccharide covered superparamagnetic oxide colloids. U.S. Patent, 526176; 1993.

22. Papisov MI, Bogdanov Jr A, Schaffer B, Nossiff N, Shen T, Weissleder R, Brady TJ. Colloidal magnetic resonance contrast agents: effect of particle surface on biodistribution. J Magnetism Magn Mater 1993;122:383–386.

23. Dodd SJ, Williams M, Suhan JP, Williams DS, Koretsky AP, Ho C. Detection of single mammalian cells by high-resolution magnetic resonance imaging. Biophys J 1999;76:103–109.

24. Haase A. Snapshot FLASH MRI. Applications to T1, T2, and chemical-shift imaging. Magn Reson Med 1990;13:77–89.

25. Weissleder R, Stark DD, Engelstad BL, Bacon BR, Compton CC, White DL, Jacobs P, Lewis J. Superparamagnetic iron oxide: pharmacokinetics and toxicity. Am J Roentgenol 1989;152:167–173.

26. Vaseghi SV. Advanced digital signal processing and noise reduction. Chichester: John Wiley & Sons; 2000. p 227–230.

27. Oppenheim AV, Schafer RW, Buck JR. Discrete-time signal processing. New Jersey: Prentice Hall; 1999. p 241–311.

28. Broersen PMT. Finite sample criteria for autoregressive order selection. IEEE Trans Signal Process 2000;48:3550–3558.

29. Kay SM. Modern spectral estimation: theory and application. New Jersey: Prentice Hall; 1987. p 228–232.

30. Golub GH, Van Loan CF. Matrix computations. Baltimore: Johns Hopkins University Press; 1996. p 75–79.

31. Zhang Y, Dodd SJ, Hendrich KS, Williams M, Ho C. Magnetic resonance imaging detection of rat renal transplant rejection by monitoring macrophage infiltration. Kidney Int 2000;58:1300–1310.

32. Chambon C, Clement O, Le Blanche A, Schouman-Claeys E, Frija G. Superparamagnetic iron oxides as positive MR contrast agents: in vitro and in vivo evidence. Magn Reson Imaging 1993;11:509–519.

33. Gore JC, Majumdar S. Measurement of tissue blood flow using intravascular relaxation agents and magnetic resonance imaging. Magn Reson Med 1990;14:242–248.

34. Trillaud H, Grenier N, Degreze P, Louail C, Chambon C, Franconi JM. First-pass evaluation of renal perfusion with TurboFLASH MR imaging and superparamagnetic iron oxide particles. J Magn Reson Imaging 1993;3:83–91.

35. Sharma RK, Gupta RK, Poptani H, Pandey CM, Gujral RB, Bhandari M. The magnetic resonance renogram in renal transplant evaluation using dynamic contrast-enhanced MR imaging. Transplantation 1995;59:1405–1409.

36. Hauger O, Delalande C, Trillaud H, Deminiere C, Quesson B, Kahn H, Cambar J, Combe C, Grenier N. MR imaging of intrarenal macrophage infiltration in an experimental model of nephrotic syndrome. Magn Reson Med 1999;41:156–162.

37. Laissy JP, Benderbous S, Idee JM, Chillon S, Beaufils H, Schouman-Claeys E. MR assessment of iodinated contrast-medium-induced nephropathy in rats using ultrasmall particles of iron oxide. J Magn Reson Imaging 1997;7:164–170.